JCTC Journal of Chemical Theory and Computation

Article

pubs.acs.org/JCTC

Spin−Orbit Coupling and Potential Energy Functions of Ar_2^+ and Kr_2^+ by High-Resolution Photoelectron Spectroscopy and *ab Initio* Quantum Chemistry

R. Mastalerz, O. Zehnder, M. Reiher,* and F. Merkt*

Laboratorium für Physikalische Chemie, ETH Zurich, 8093 Zurich, Switzerland

ABSTRACT: The dependence of the spin−orbit-coupling constant of the six low-lying electronic states of Ar_2^+ and Kr_2^+ on the internuclear distance R has been calculated *ab initio*. The spin−orbit-coupling constant varies by about 10% over the range of internuclear distances relevant for the interpretation of the high-resolution photoelectron spectra of Ar_2 and Kr_2 and can be accurately represented by a Morse-type function for the states of *ungerade* electronic symmetry and by an exponentially decreasing function for the states of *gerade* symmetry. The spin−orbit-coupling constant is larger than the asymptotic value (at $R \rightarrow \infty$) for the *gerade* states and smaller for the *ungerade* states. The calculated R-dependent spin−orbit-coupling constants were used to derive a new set of potential energy functions for the low-lying electronic states of Ar_2^+ and Kr_2^+ and to quantify the errors resulting from the widely used approach consisting of approximating the spin−orbit-coupling constant by its asymptotic value. The effects of the R dependence on the potential energy functions of the six low-lying electronic states of the homonuclear rare-gas dimer ions are found to be very small for Ar_2^+ (and by inference also for Ne_2^+) but significant for Kr_2^+. The shifts arising in calculations of the potential energy functions from a neglect of the R dependence of the spin−orbit-coupling constant are the result of the interplay between the differences between the binding energies of the relevant $^2\Pi$ and $^2\Sigma^+$ states, the magnitude of the spin−orbit-coupling constant, and the magnitude and sign of the deviations between the R-dependent spin−orbit-coupling constant and its asymptotic value at large internuclear distances.

I. INTRODUCTION

The singly charged homonuclear rare-gas dimer ions Rg_2^+ (Rg = Ne, Ar, Kr, and Xe) possess six low-lying electronic states, three of *gerade* (g) and three of *ungerade* (u) electronic symmetry. At short internuclear distances, Hund's angular momentum coupling cases a and b provide an adequate description of these states, which are labeled A $^2\Sigma_u^+$, B $^2\Pi_{\Omega,g}$, C $^2\Pi_{\Omega,u}$, and D $^2\Sigma_g^+$ (Ω = 1/2 and 3/2) in the notation used by Mulliken.[1] These states result from the removal of an electron out of one of the outer-valence-shell molecular orbitals $p\sigma_u$, $p\pi_g$, $p\pi_u$, and $p\sigma_g$ that are formed by a linear combination of the atomic valence np orbitals (n = 2, 3, 4, and 5 for Ne, Ar, Kr, and Xe, respectively). In Hund's case c angular momentum coupling scheme, which is appropriate at larger internuclear distances, these states are denoted I(1/2u), I(3/2g), I(3/2u), I(1/2g), II(1/2u), and II(1/2g), where the half-integer number represents the quantum number Ω associated with the projection of the total (spin and orbital) electronic angular momentum onto the internuclear axis, and I and II designate states correlating adiabatically to the $Rg(^1S_0) + Rg^+(^2P_{3/2})$ and $Rg(^1S_0) + Rg^+(^2P_{1/2})$ dissociation limits, respectively. Whereas the Ω = 3/2 states have pure Π electronic character, the Ω = 1/2 states have mixed Σ and Π character. The degree of mixing increases with increasing internuclear separation because, at large separation, the spin−orbit interaction becomes stronger than the interatomic interactions and decouples the electronic orbital motion from the internuclear axis.

The quantitative description of these low-lying electronic states in terms of potential energy functions is of practical importance for the characterization of the physical and chemical processes (e.g., charge-exchange[2] and scattering[3] processes) taking place in rare-gas plasmas, such as those arising in excimer lasers,[4,5] rare-gas lamps,[6] rare-gas ion lasers,[7] and electric space-propulsion thrusters. The potential energy functions of the low-lying electronic states of rare-gas dimer ions are also needed to understand the photoionization dynamics of the neutral rare-gas dimers (see, e.g., refs 8 and 9), to model the electronically excited (Rydberg) states of Rg_2[10] and the structure and fragmentation dynamics of larger rare-gas cluster ions.[11−13]

In past decades, a considerable body of information on the low-lying electronic states of Rg_2^+ has been obtained from electronic-structure calculations (see, in particular, refs 14−30); from experiments, primarily photoelectron, photoionization, and electron impact ionization spectroscopy[31−53] (including measurements of photofragment kinetic energy distributions[8,9,54]); and from a combination of experiment and theory.[55,56]

Until recently, almost all derivations of the potential energy functions of the six low-lying electronic states of Rg_2^+, be it from *ab initio* calculations or from experimental data, have relied on a potential model introduced by Cohen and Schneider[57] and characterized by two separate spin−orbit-interaction matrices of the form presented in Table 1, one for the three g and one for the three u states. This potential model relies on several assumptions and approximations

Special Issue: Wilfred F. van Gunsteren Festschrift

Received: January 31, 2012
Published: April 6, 2012

Table 1. Spin-Orbit Interaction Matrix in Hund's Case a Basis Describing the Coupling between the States of $^2\Sigma^+$ and $^2\Pi$ Symmetry in the Homonuclear Rare-Gas Dimer Ions

	$^2\Sigma_{1/2}{}^+$	$^2\Pi_{1/2}$	$^2\Pi_{3/2}$
$^2\Sigma_{1/2}{}^+$	$V_\Sigma(R)$	$-a(R)/\sqrt{2}$	
$^2\Pi_{1/2}$	$-a(R)/\sqrt{2}$	$V_\Pi(R) + a(R)/2$	
$^2\Pi_{3/2}$			$V_\Pi(R) - a(R)/2$

(see ref 58 for a detailed discussion), the most important of which is the assumption that the spin–orbit-coupling constant a does not depend on the internuclear separation and equals $a_{Rg^+} = 2A_{Rg^+}/3$, where A_{Rg^+} represents the separation between the $^2P_{1/2}$ and the $^2P_{3/2}$ spin–orbit components of the ground state of Rg^+. The sign of the spin–orbit-coupling constant a_{Rg^+} of Rg^+ is negative so that, strictly, $2A_{Rg^+}/3 = -a_{Rg^+}$. The form of the spin–orbit-coupling matrix given in Table 1 assumes a positive value of $a(R)$, which must therefore be interpreted as the absolute value of the spin–orbit-coupling constant. We adopt this convention here to be consistent with earlier work on the potential energy functions of the rare-gas dimer ions.[15,24,28]

In the case of Xe_2^+, we have recently calculated the R dependence of a and established that a varies by about 10% over the range of internuclear separation for which experimental observations are available.[56] Beyond R = 2 Å, the calculated spin–orbit-coupling functions $a_{g,u}(R)$ for the g and u states could be represented accurately by simple analytical functions, a Morse-type function for the u states and an exponentially decaying function for the g states (see eqs 5 and 6 below). The calculated functions $a(R)$ were used to determine a new set of potential energy functions for the six low-lying electronic states of Xe_2^+ in a least-squares fit to high-resolution photoelectron spectroscopic data. The calculation enabled us to quantify the effects of the R dependence of the spin–orbit-coupling constant and led to the conclusion that it needs to be taken into account when deriving potential energy functions using Table 1 if an absolute accuracy better than 100 cm^{-1} is desired.

We present here an extension of these calculations to the low-lying electronic states of Ar_2^+ and Kr_2^+, two other homonuclear rare-gas dimer cations for which a significant spin–orbit interaction can be expected from the spin–orbit splitting A_{Rg^+} of the ^2P ground state of the atomic ion (A_{Ar^+} = 1431.5831 cm^{-1} [59] and A_{Kr^+} = 5370.294 cm^{-1} [60]). This work was carried out with the objectives of (i) determining the R dependence of the spin–orbit-coupling constants of the low electronic states of Ar_2^+ and Kr_2^+, (ii) finding out whether the R dependence of the spin–orbit-coupling constant can be described by analytical functions of the same type as in the case of Xe_2^+, (iii) quantifying possible effects of this R dependence on the potential energy functions, and (iv) deriving an improved set of potential energy functions for Ar_2^+ and Kr_2^+ using the calculated spin–orbit-coupling constants in a least-squares fit to available spectroscopic data.

The structure of the article is as follows: After a presentation of the model employed to determine the potential energy functions of the six low-lying electronic states in section II, the computational methods used to calculate the R-dependent spin–orbit-coupling constant are recapitulated in section III. The experimental data used to derive the potential energy functions of Ar_2^+ and Kr_2^+ are then summarized in section IV. The results of the least-squares fit are presented in section V, where they are compared with the experimental data.

II. POTENTIAL MODEL

The method used to determine the potential energy functions of the six low-lying electronic states of Ar_2^+ and Kr_2^+ relies on the treatment of the spin–orbit interaction by means of the Hamiltonian matrix given in Table 1. The electronic energies of these states correspond to the eigenvalues of the matrix and are determined as functions of the internuclear distance R. The method is semiempirical in nature: It relies on the determination of the R-dependent spin–orbit-coupling constants $a(R)$ by computational methods as described in section III and on model analytic functions for the potential energy functions V_Σ and V_Π, the parameters of which are determined in least-squares fits to experimental data. The treatment of the spin–orbit interaction corresponds to that introduced by Cohen and Schneider[57] but is improved by the use of R-dependent spin–orbit-coupling functions.

Because the spin–orbit operator only couples states of the same g/u symmetry, two distinct 3 × 3 matrices are set up, one for the g states, the other for the u states. The spin–orbit-interaction matrices are expressed in the basis set adequate for the short-range part of the potentials in which the quantum numbers Λ, Σ, and Ω = Λ + Σ corresponding to, respectively, the projection of the total orbital, total electron spin, and total electronic angular momenta onto the internuclear axis are good quantum numbers. Consequently, the electronic potential energies of the $^2\Sigma_{1/2}{}^+$, $^2\Pi_{1/2}$, and $^2\Pi_{3/2}$ states appear as diagonal elements in the matrix displayed in Table 1. The spin–orbit-coupling operator is not only described by diagonal (first-order) contributions of $\pm a(R)/2$, which induce a splitting of the $^2\Pi$ state into the two components $^2\Pi_{1/2}$ and $^2\Pi_{3/2}$, but also by off-diagonal (second-order) elements $-a(R)/\sqrt{2}$, which couple states of the same value of Ω, namely, the $^2\Sigma_{1/2}{}^+$ and $^2\Pi_{1/2}$ states.[57,58]

The potential energy functions of the $^2\Sigma^+$ and $^2\Pi$ states under neglect of the spin–orbit interaction are expressed as[49]

$$V_\Lambda(R) = A_\Lambda\, e^{-b_\Lambda R} - B_\Lambda\, e^{-b_\Lambda R/\beta_\Lambda} - \sum_{n=2}^{3} f_{2n}(R, b_\Lambda)\frac{C_{2n,\Lambda}}{R^{2n}} + V_{diss} \quad (1)$$

with Λ = Σ, Π. The first, second, and third terms on the right-hand side of eq 1 describe the repulsive interaction at short range, the chemical bonding at intermediate internuclear distances, and the dominant members of the Tang–Toennies long-range interaction series,[61] respectively. V_{diss} is a constant used to relate the potential energies to the energy of the X 0_g^+ ($v'' = 0$) ground neutral state and is defined as

$$V_{diss} = D_0(Rg_2, X\ 0_g^+) + E_i(Rg, {}^2P_{3/2} \leftarrow {}^1S_0)/hc + \frac{a_{Rg^+}}{2} \quad (2)$$

where $D_0(Rg_2, X\ 0_g^+)$ represents the dissociation energy of the ground state neutral rare-gas dimer, $E_i(Rg, {}^2P_{3/2} \leftarrow {}^1S_0)$ is the first ionization energy of the neutral rare-gas atom, and $a_{Rg^+} = 2A_{Rg^+}/3$.

After determining the potential energy functions $V_j(R)$ of the three u and three g states as eigenvalues of the interaction matrix presented in Table 1 for a given set of parameters in eq 1, the calculated positions of the vibrational levels of the

dx.doi.org/10.1021/ct300078m | J. Chem. Theory Comput. 2012, 8, 3671–3685

electronic state j are obtained by numerically solving the one-dimensional Schrödinger equation

$$\left[-\frac{\hbar^2}{2\mu_i}\frac{d^2}{dR^2} + hc\, V_j(R)\right]\psi_{ijv}(R) = E_{ijv}\,\psi_{ijv}(R) \tag{3}$$

corresponding to the vibrational motion of the isotopomer with reduced mass μ_i in the potential $V_j(R)$ following the procedure described in refs 40 and 49. In eq 3, the indices i and v designate the isotopomer and the vibrational quantum number of the ion, respectively.

The optimal set of parameters determining the functions $V_{\Sigma_u}(R)$, $V_{\Pi_u}(R)$, $V_{\Sigma_g}(R)$, and $V_{\Pi_g}(R)$ are derived by minimizing the deviations between calculated and experimental level positions in a least-squares-fit procedure. The majority of the potential parameters in eq 1 are known with sufficient accuracy from experimental results or theory that they do not need to be optimized, as will be discussed further in section V.

III. COMPUTATIONAL DETAILS

The computational methodology used to obtain the spin−orbit-coupling constant of the lowest-lying Σ and Π states of *gerade* and *ungerade* symmetry in Ar_2^+ and Kr_2^+ has already been applied to Xe_2^+ as described in ref 56. Consequently, only aspects specific to Ar_2^+ and Kr_2^+ are summarized here, and we refer to ref 56 for additional information. The spin−orbit-coupling constant was obtained from *ab initio* data by exploiting the block-diagonal form of the spin−orbit-interaction matrix presented in Table 1, which allows a calculation of $a(R)$ at a specific internuclear distance R from

$$a(R) = 2(E_{el}^{\Pi}(R) - E_{el}^{\Pi_{3/2}}(R)) \tag{4}$$

where $E_{el}^{\Pi}(R)$ corresponds to the electronic energies of the $^2\Pi$ states without consideration of the spin−orbit interaction and $E_{el}^{\Pi_{3/2}}(R)$ to the energies of the $^2\Pi_{3/2}$ electronic states which are equivalent to the I(3/2u or g) states within the approximations implied by Table 1.

Davidson-corrected multireference configuration interaction all-electron calculations with singles and doubles excitations (MRCISD+Q) were performed employing the scalar-relativistic second-order Douglas−Kroll−Hess (DKH) Hamiltonian[62] in combination with the ANO-RCC basis sets of Roos et al.[63] The basis sets were used in a fully decontracted form, resulting in the overall sizes of (17s/12p/5d/4f/2g) in the case of Ar and (20s/17p/11d/4f/2g) in the case of Kr. A total of 35 electrons were explicitly correlated in the MRCISD+Q calculations, corresponding to the 1s, 2s, 2p, 3s, and 3p shells of Ar and the 3d, 4s, and 4p shells of Kr. The spin−orbit interaction was considered as a perturbation and treated in an *a posteriori* procedure.

The energies of the six lowest-lying Hund's-case-c-coupled states, in particular the energy $E_{el}^{\Pi_{3/2}}$ of the $^2\Pi_{3/2}$ state that is needed to evaluate eq 4, were obtained from a state-interaction approach by diagonalizing the matrix representation of the electronic Hamiltonian and the spin−orbit Hamiltonian in the basis of the eigenfunctions of the electronic Hamiltonian. The spin−orbit matrix was constructed in a truncated basis set ((17s/12p/5d) for Ar and (20s/17p/11d) for Kr). Its elements were set up from the spin−orbit part of the Breit−Pauli Hamiltonian in the case of internal configurations, whereas an effective mean-field Fock operator[64] was employed for external configurations. All diagonal elements of the resulting spin−orbit matrix, however, were shifted in energy to correspond to the MRCISD+Q energies obtained with the complete decontracted basis sets. The MRCI calculations were performed with the MOLPRO2002.6 program suite.[65] The potential energy curves were determined for internuclear distances ranging from 3.5 to 14.0 a_0 in the case of Kr_2^+ and 2.5 to 10.0 a_0 in the case of Ar_2^+ (a_0 is the Bohr radius).

The R dependences of the spin−orbit-coupling constants calculated for Ar_2^+ and Kr_2^+ are depicted in Figure 1 where

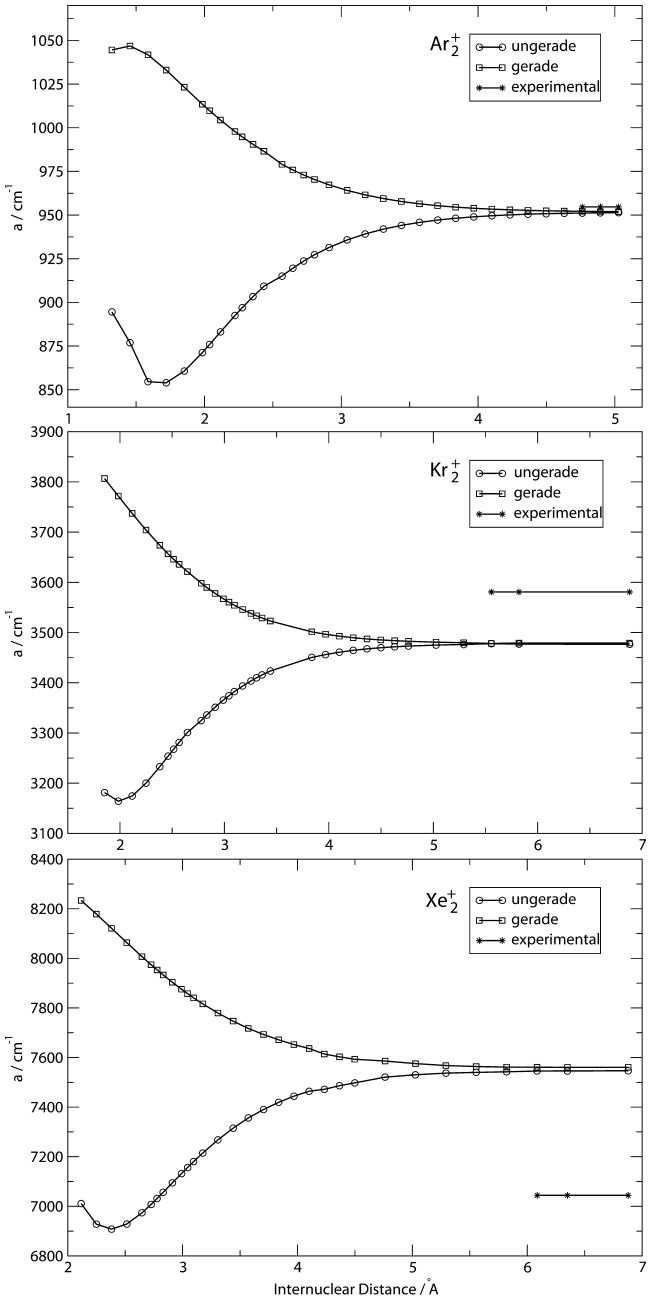

Figure 1. The spin−orbit coupling constant $a(R)$ in Ar_2^+, Kr_2^+ (this work), and Xe_2^+ (from ref 56) obtained from Davidson-corrected DKH2 MRCISD calculations. The horizontal lines at large distances mark the position of asymptotic value of the spin−orbit-coupling constants determined by atomic spectroscopy, which have been taken from refs 59 and 75 (Ar^+), 60 and 76 (Kr^+), and 77 (Xe^+).

they are compared with the results obtained previously for Xe_2^+ [56] and with the experimental values of the asymptotic

dx.doi.org/10.1021/ct300078m | J. Chem. Theory Comput. 2012, 8, 3671−3685

Table 2. Comparison of the Parameters Describing $a(R)$ for Ar_2^+, Kr_2^+, and Xe_2^+

	u states			*g* states		
	Ar_2^+	Kr_2^+	Xe_2^+	Ar_2^+	Kr_2^+	Xe_2^+
a_0/cm^{-1}	97.5	325.0	597.2	122.9	756.5	1084.5
a_1	1.688	1.636	1.566	0.094	0.230	0.086
a_2	1.632	1.990	2.359	2.902	2.015	2.500

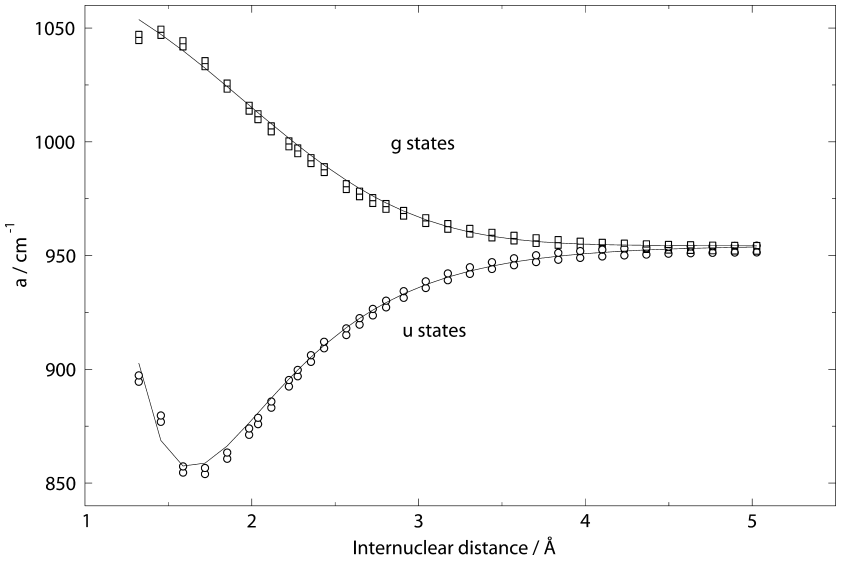

Figure 2. *R*-dependent spin−orbit-coupling constant $a(R)$ for the *u* (circles) and the *g* (squares) states of Ar_2^+ derived from DKH2 MRCI+Q *ab initio* calculations (open circles and squares). The filled circles and squares are scaled such that the asymptotic value is equal to the spin−orbit splitting of the Ar^+ ^2P ground state. The full lines represent fits based on the expressions in eqs 5 and 6. The data for Xe_2^+ are from ref 56.

spin−orbit-coupling constants *a* calculated from $a_{Rg^+} = 2A_{Rg^+}/3$, where *A* denotes the energy splitting between the $^2P_{1/2}$ and $^2P_{3/2}$ states of the corresponding rare-gas atomic ion. As already noticed in the case of Xe_2^+, the *R*-dependent spin−orbit-coupling functions of the *g* and *u* states follow a different pattern at short internuclear distances: $a_u(R)$ drops significantly below the asymptotic value, whereas $a_g(R)$ becomes significantly larger than $2A_{Rg^+}/3$. In the vicinity of the dissociation limit of Ar_2^+ (i.e., for $R\rightarrow\infty$), the theoretical value of *a* agrees with the experimental value within better than 3 cm^{-1}, which represents a deviation of only 0.3% (see top panel of Figure 1). In the case of Kr_2^+ (middle panel of Figure 1), the MRCISD+Q spin−orbit calculations predict the asymptotic value of *a* to be approximately 100 cm^{-1} (i.e., about 2.8%) less than the experimental value. The deviation between calculated and experimental values of the asymptotic spin−orbit-coupling constant is largest in the case of Xe_2^+ (bottom panel of Figure 1), the calculations overestimating it by about 500 cm^{-1}, or almost 7%.[56]

The decrease of the accuracy of the calculations of the spin−orbit-coupling functions from Ar_2^+ to Xe_2^+ that is betrayed by the increasing deviation between computed and experimental asymptotic values has two main causes: The first is related to the decreasing quality of the electron-correlation treatment in the MRCISD+Q calculations. In the MRCISD+Q calculation on Ar_2^+, no frozen-core approximation was needed, because all electrons could be explicitly included in the electron-correlation procedure, which resulted in accurate unperturbed wave functions for the subsequent spin−orbit calculation. In contrast, the MRCISD+Q calculations on the heavier dimer ions had to be performed with a predefined frozen core of 36 and 72 (noncorrelated) electrons in the cases of Kr_2^+ (total number of electrons: 71) and Xe_2^+ (total number of electrons: 107, see ref 56), respectively. The resulting unperturbed wave functions are therefore less accurate than in the case of Ar_2^+. The second cause is the increasing magnitude of the spin−orbit interaction combined with the fact that the interaction is treated as a first-order perturbation in the subsequent state-interaction approach. This combination inevitably results in a loss of accuracy.

The derivation of the potential energy functions by the least-squares fit procedure described in section II requires the matrix elements of Table 1 to be expressed in analytical form. In the range of internuclear distances relevant to the experimental observations, the spin−orbit-coupling constants a_g and a_u of the *gerade* and *ungerade* states can be almost perfectly described by the expressions

$$a_u(R) = a_{Rg^+} - a_{u,0}(1 - [1 - \exp(-a_{u,1}(R/\text{Å} - a_{u,2}))]^2) \quad (5)$$

and

$$a_g(R) = a_{Rg^+} + a_{g,0}\exp(-a_{g,1}(R/\text{Å})^{a_{g,2}}) \quad (6)$$

respectively, in which $a_{Rg^+} = 2A_{Rg^+}/3$ represents the asymptotic value (Rg = Ar, Kr). Equation 5 is a Morse-type function, and eq 6 falls exponentially with increasing *R* value. In order to derive as accurate spin−orbit-coupling functions as possible from the *ab initio* calculations, the following two-step procedure was followed: First, the computed constants were scaled linearly so that the asymptotic value exactly matched the experimental value determined by atomic spectroscopy, i.e., $a(R \rightarrow \infty) = 2A_{Rg^+}/3$, with $A_{Rg^+} = [E(Rg^+,^2P_{1/2}) - E(Rg^+,^2P_{3/2})]/hc$. Then,

dx.doi.org/10.1021/ct300078m | J. Chem. Theory Comput. 2012, 8, 3671−3685

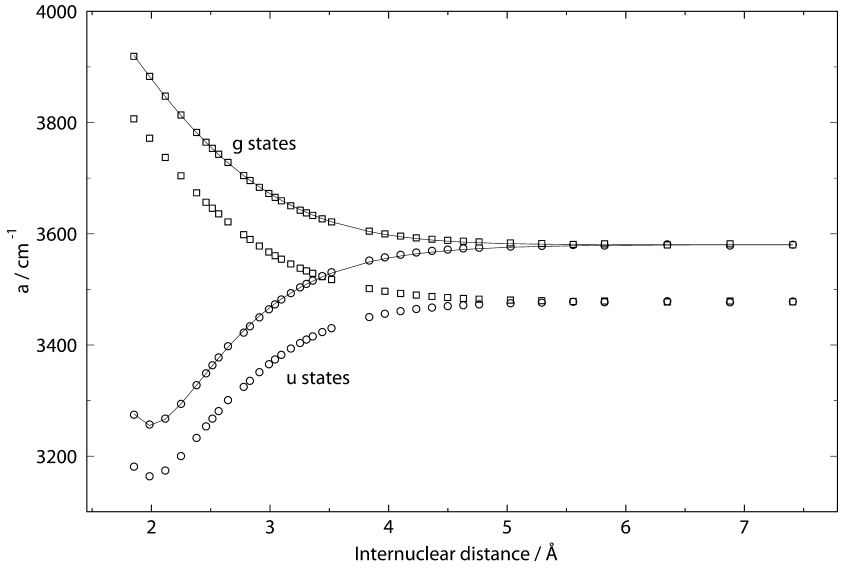

Figure 3. *R*-dependent spin−orbit-coupling constant $a(R)$ for the *u* (circles) and the *g* (squares) states of Kr_2^+ derived from DKH2 MRCI+Q *ab initio* calculations (open circles and squares). The filled circles and squares are scaled such that the asymptotic value is equal to the spin−orbit splitting of the Kr^+ ^2P ground state. The full lines represent fits based on the expressions in eqs 5 and 6.

the parameters $a_{u,i}$ and $a_{g,i}$ (i = 0, 1, 2) were determined from the scaled *ab initio* data in a least-squares-fit procedure. The optimal parameters $a_{u,i}$ and $a_{g,i}$ (i = 0, 1, 2) are listed in Table 2, where they are compared with the values determined for Xe_2^+ in ref 56.

This two-step procedure is illustrated in Figures 2 and 3 for Ar_2^+ and Kr_2^+, respectively, where the open circles and squares represent the values calculated *ab initio*; the full circles and squares, the scaled spin−orbit-coupling constants with correct asymptotic value; and the full lines, the results of least-squares fits based on eqs 5 and 6.

The spin−orbit-coupling functions presented in Table 2 and Figures 2 and 3 represent the main results of the computational part of this article. The fact that eqs 5 and 6 perfectly describe the shape of the calculated spin−orbit-coupling functions of all three dimer ions makes us confident that these functions are well suited to describe the *R* dependence of the spin−orbit-coupling constants in these molecules and related molecular systems such as Y_2^- (Y = F, Cl, Br, and I). Because of the semiempirical nature of the scaling procedure, we further expect these functions to describe the *R* dependence of a_g and a_u sufficiently accurately so that they can be held fixed when deriving the potential energy functions from experimental data using the matrix presented in Table 1.

IV. EXPERIMENTAL DATA

The experimental data used to derive the potential energy functions of the six low-lying electronic states of Ar_2^+ and Kr_2^+ stem from studies of the pulsed-field-ionization zero-kinetic-energy (PFI-ZEKE) photoelectron spectra of Ar_2[39,40,45,46] and Kr_2.[43,44,52] Details concerning the measurement procedure, the assignment of the spectra, and the estimation of the experimental uncertainties in the spectral positions have been given in the original publications.

In the case of Ar_2^+, the data set consists of the positions of the I(1/2 *u*, v^+ = 3, 5−10, 12−50), I(3/2 *u*, v^+ = 0), and II(1/2 *u*, v^+ = 0−2) levels of $^{40}Ar_2^+$ and the I(1/2 *u*, v^+ = 20, 21) levels of $^{36}Ar_2^+$ measured by single-photon PFI-ZEKE photoelectron spectroscopy,[39,40] and of the I(1/2 *u*, v^+ = 35−50), I(3/2 *g*, v^+ = 0−10), I(3/2 *u*, v^+ = 0−2), I(1/2 *g*, v^+ = 1−5), and II(1/2 *u*, v^+ = 0−2) levels of $^{40}Ar_2^+$ and the I(1/2 *u*, v^+ = 38−46), I(3/2 *g*, v^+ = 0−7), I(3/2 *u*, v^+ = 0−2), I(1/2 *g*, v^+ = 3, 4), and II(1/2 *u*, v^+ = 0−2) levels of $^{36}Ar_2^+$, all measured with rotational resolution by (1 + 1′) resonance-enhanced two-photon excitation via selected rovibrational levels of the 0_u^+ level of Ar_2 located below the Ar 4s[1/2]$_1$ + Ar $^1S_0$ dissociation threshold.[45,46] These data were summarized in ref 49 and employed to extract potential energy functions of the six low-lying electronic states of Ar_2^+ in a global fit based on the assumption of an *R*-independent spin−orbit-coupling constant.

In the case of Kr_2^+, the data set consists of the positions of the I(1/2 *u*, v^+ = 0, 1, 5, 6, 15−18, 20, 22, 24−29, 32, 33,

Table 3. Parameters of the Interaction Potentials of the Lowest Electronic States of Ar_2^+ [a]

	u states		*g* states	
	$^2\Sigma_u^+$	$^2\Pi_u$	$^2\Sigma_g^+$	$^2\Pi_g$
$R_{e,\Lambda}$/Å	2.41739 ± 0.00037	3.82765 ± 0.00063	5.3967 ± 0.0070	3.0101 ± 0.0024
$D_{e,\Lambda}$/cm^{-1}	11219.8 ± 1.5	332.633 ± 0.099		1561.83 ± 0.48
β_Λ	1.44268 ± 0.00032	1.4242 ± 0.0016		1.4486 ± 0.0031
b_Λ/Å^{-1}	2.75839 ± 0.00038	2.9639 ± 0.0011	2.1709 ± 0.0025	3.1681 ± 0.0029
$C_{4,\Lambda}$/(cm^{-1} Å^4)[b,c]	95302	95302	95302	95302
$C_{6,\Lambda}$/(cm^{-1} Å^6)[b,c]	511433	243089	511433	243089
A_Λ/cm^{-1} [d]	1.832 × 10^7	1.741 × 10^7	5.720 × 10^6	3.157 × 10^7
B_Λ/cm^{-1} [d]	3.154 × 10^6	79800		1.772 × 10^6
RMS	0.84		0.75	
		$a_u(R)$		$a_g(R)$
a_{Ar^+}/cm^{-1}		954.3887[b,e]		954.3887[b,e]
a_0/cm^{-1}		97.5[b]		122.9[b]
a_1		1.688[b]		0.094[b]
a_2		1.632[b]		2.902[b]

[a]The uncertainties represent 95% confidence intervals. Parameters given without uncertainties were held fixed. [b]This parameter was kept constant during the fit. [c]Values from refs 66 and 67. [d]Determined from $R_{e,\Lambda}$ and $D_{e,\Lambda}$ using eqs 7 and 8. [e]Value from ref 59.

dx.doi.org/10.1021/ct300078m | J. Chem. Theory Comput. 2012, 8, 3671−3685

Table 4. Dissociation Energies D_e and Equilibrium Internuclear Distances R_e of the Lowest Six Electronic States of Ar_2^+ Determined from the Potential Energy Curves Displayed in Figures 4 and 5

			I(1/2g)[a]					
	I(1/2u)	I(3/2g)	inner	outer well	I(3/2u)	II(1/2u)	II(1/2g)	reference
D_e/cm^{-1}	10761.8	1568.0	659.2	115.0	330.3	652.4	181.8	this work
	10759	1568	665	113	330	651	177	49
	10778	1434	549	79	283	590	134	29
	10769	1744	849		357	687	66	24
R_e/Å	2.418	3.008	3.027	4.871	3.832	3.673	4.517	this work
	2.423	2.996	3.010	4.908	3.805	3.653	4.541	49
	2.4047	3.0242	3.0449	5.2745	3.8783	3.6979	4.6865	29
	2.410	2.945	2.957		3.708	3.606	4.699	24

[a]There is a local maximum on the potential energy curve at R_{max} = 4.076 Å and $V(R_{max}) = E(Ar(^1S_0) + Ar^+(^2P_3 = 2)) - 75.0$ cm^{-1}.

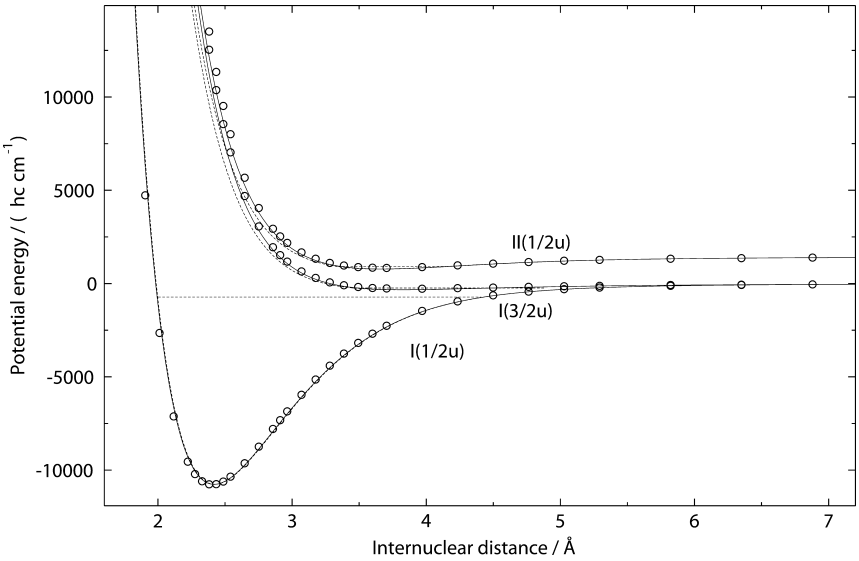

Figure 4. Comparison of the potential energy functions of the I(1/2u), I(3/2u), and II(1/2u) states of Ar_2^+ derived in this work (full line), in ref 49 (dashed line) and in ref 29 (circles). The dashed horizontal lines indicate for each state the positions of the highest observed vibrational level.

35−53), I(3/2 u, v^+ = 0−2), and II(1/2 u, v^+ = 0−8) levels of several isotopomers of Kr_2^+ determined by single-photon PFI-ZEKE photoelectron spectroscopy,[43] and the positions of the I(1/2 u, v^+ = 55−60, 62−67, 69, 73, 74), I(3/2 u, v^+ = 0−10), and II(1/2 u, v^+ = 0−8) levels of $^{84}Kr_2^+$, and of the I(1/2 u, v^+ = 56−60), I(3/2 u, v^+ = 0−6), and II(1/2 u, v^+ = 3−9) levels of $^{86}Kr^{84}Kr^+$ measured by PFI-ZEKE photoelectron spectroscopy following (2 + 1′) resonant three-photon excitation via the 0_g^+ Rydberg state of Kr_2 located below the Kr 5p[1/2]$_0$ + Kr $^1S_0$ dissociation threshold.[44,52] Because of the small rotational constants of Kr_2 and Kr_2^+, the rotational structure of the PFI-ZEKE photoelectron spectra could not be resolved. The positions of the ionic vibrational levels with respect to that of the neutral ground state were therefore assumed to correspond to the maximum of the smooth intensity distributions resulting from the unresolved rotational structure of the relevant bands. Possible errors induced by this procedure were included in the experimental uncertainties. The observed spectral positions $\tilde{\nu}_{obs}$ and their experimental uncertainties are summarized in Tables 7−11 for Ar_2^+ and Tables 12−14 for Kr_2^+ (see Appendix), where they are compared with the positions calculated from the potential energy functions determined in this work, as explained in the next section.

The experimental data set just described contains information on all low-lying electronic states of Ar_2^+ and Kr_2^+ except the II(1/2g) state of Ar_2^+ and the I(1/2g) and II(1/2g) states of Kr_2^+. These three states are very weakly bound, and attempts at observing their (ro)vibrational energy level structure have remained unsuccessful so far. Because the spin−orbit-coupling matrix (Table 1) necessitates the knowledge of at least two of the three states of g or u symmetry, the experimental data on Ar_2^+ are sufficient, in combination with the calculated R-dependent spin−orbit-coupling matrix, to extract the potential energy functions of all six low-lying states and to estimate the positions of the so far unobserved vibrational levels of the II(1/2g) state. The potential energy functions of the g states of Kr_2^+, however, cannot be determined from the experimental data set.

V. THE POTENTIAL ENERGY FUNCTIONS OF THE LOW-LYING ELECTRONIC STATES OF Ar_2^+ and Kr_2^+

One of the major advantages of the procedure described in section II to determine the potential energy functions of the low-lying electronic states of the rare-gas-dimer ions from experimental data, next to the fact that it includes the R dependence of the spin−orbit-coupling constant, is the small number of potential parameters that need to be optimized. The three coupled potential functions can be obtained by adjusting only eight parameters (the coefficients A_Λ, B_Λ, b_Λ, and β_Λ for

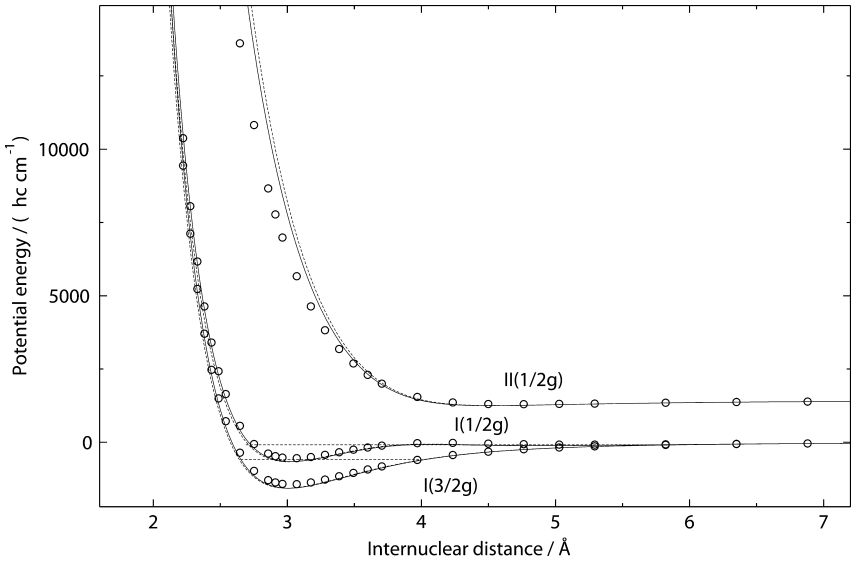

Figure 5. Comparison of the potential energy functions of the I(3/2*g*), I(1/2*g*), and II(1/2*g*) states of Ar_2^+ derived in this work (full line), in ref 49 (dashed line) and in ref 29 (circles). The dashed horizontal lines indicate for each state the positions of the highest observed vibrational level.

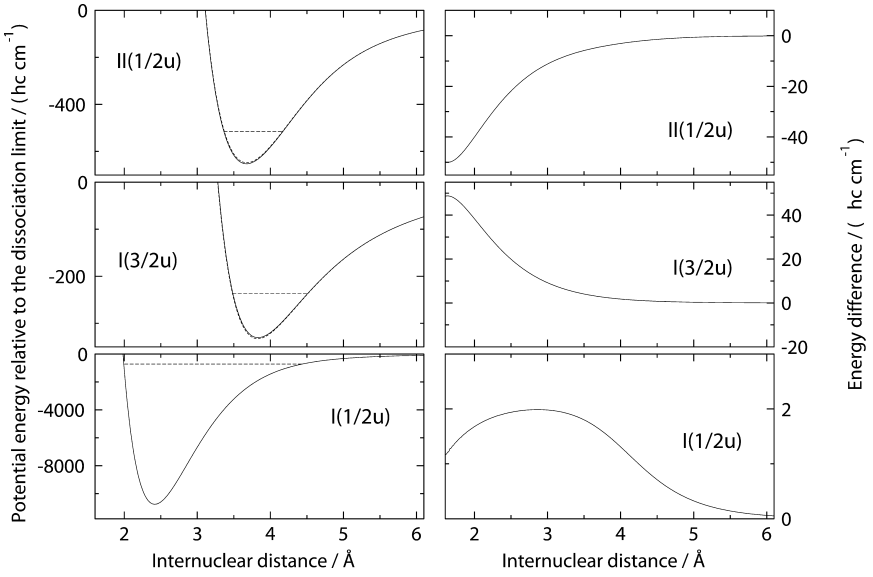

Figure 6. Left panels: Potential energy functions of the I(1/2*u*) (bottom), I(3/2*u*) (middle), and II(1/2*u*) (top) states of Ar_2^+ calculated with *R*-dependent $a_u(R)$ (full lines) and *R*-independent $a = a_{Ar+}$ (dashed lines) using the same Σ and Π potential energy curves (parameter set for the *u* states in Table 3). The dashed horizontal lines indicate for each state the positions of the highest observed vibrational level. Right panels: Energy difference of the two curves displayed in the left panels for the I(1/2*u*) (bottom), I(3/2*u*) (middle), and II(1/2*u*) (top) states of Ar_2^+.

Λ = Σ and Π) for the *u* states and seven for the *g* states. Indeed, the second term in eq 1, which describes the chemical bond, can be neglected for the $^2\Sigma_g^+$ state ($B_{\Sigma_g} = 0$) because it is only very weakly bound. Rather than optimizing the parameters A_Λ and B_Λ, it turned out to be advantageous to optimize the equilibrium distance R_e and the dissociation energy D_e with which A_Λ and B_Λ can be calculated using the conditions (see Appendix A of ref 49)

$$\left.\frac{dV_\Lambda(R)}{dR}\right|_{R=R_{e,\Lambda}} = 0 \tag{7}$$

and

$$V_\Lambda(R_{e,\Lambda}) = V_{diss} - D_{e,\Lambda} \tag{8}$$

The coefficients $C_{2n,\Lambda}$ of the Tang–Toennies long-range expansion series[61] were taken from refs 52, 66, and 67. The values of $V_{diss}(^{40}Ar_2)$ = 127671.48 cm^{-1}, $V_{diss}(^{36}Ar_2)$ = 127670.686 cm^{-1}, and $V_{diss}(Kr_2)$ = 118411.5 cm^{-1} were obtained from the literature values $a_{Ar^+} = 2A_{Ar^+}/3$ = 954.3887 cm^{-1},[59] $a_{Kr^+} = 2A_{Kr^+}/3$ = 3580.196 cm^{-1},[60] $E_i(Ar, {}^2P_{3/2})/hc$ = 127109.842 cm^{-1},[68] $E_i(Kr, {}^2P_{3/2})/hc$ = 112914.434 cm^{-1},[69] $D_0(^{40}Ar_2, X\ 0_g^+)$ = 84.44 cm^{-1}, $D_0(^{36}Ar_2, X\ 0_g^+)$ = 83.65 cm^{-1}, and $D_0(^{84}Kr–^{86}Kr, 0_g^+) \approx D_0(^{84}Kr_2, X\ 0_g^+)$ = 126.8 cm^{-1}.[70,71] The dissociation energies of the neutral Ar_2 dimers were calculated by solving the radial Schrödinger equation for the ground electronic state with the interaction potential reported by Tang and Toennies[61] using the same procedure as described in ref 72 for Ne_2.

Weighted least-squares fits of the potential parameters were carried out separately for the *u* and *g* states. The quality of the

fits was assessed from the normalized root-mean-square deviation (RMS value of the fit), which is given by $(\chi^2/n)^{1/2}$, where $n = N - P$ represents the number of degrees of freedom, i.e., the difference between the number of experimental data points N and the number of adjustable parameters P, and

$$\chi^2 = \sum_{i=1}^{N} \left(\frac{\tilde{\nu}_i^{\mathrm{obs}} - \tilde{\nu}_i^{\mathrm{calcd}}}{\sigma_i} \right)^2 \quad (9)$$

The values of the experimental uncertainties are listed with the level positions in Tables 7−14 (see Appendix), which also compare the positions of the vibrational levels of Ar_2^+ and Kr_2^+ with those calculated from the potential energy functions.

Table 5. Parameters of the Interaction Potentials of the Lowest *ungerade* Electronic States of Kr_2^+ [a]

	$^2\Sigma_u^+$	$^2\Pi_u$
$R_{e,\Lambda}$/Å	2.68256 ± 0.00022	4.13932 ± 0.00055
$D_{e,\Lambda}$/cm^{-1}	10922.54 ± 0.52	392.42 ± 0.12
β_Λ	1.37907 ± 0.00028	77.1[b]
b_Λ/Å^{-1}	2.47608 ± 0.00024	3.01931 ± 0.00045
$C_{4,\Lambda}$/(cm^{-1} Å^4)[c,d]	144025	144025
$C_{6,\Lambda}$/(cm^{-1} Å^6)[c,d]	1028937	498324
A_Λ/cm^{-1} [e]	2.000 × 10^7	5.312 × 10^7
B_Λ/cm^{-1} [e]	4.130 × 10^6	8.440
RMS	1.19	
		$a_u(R)$
a_{Kr^+}/cm^{-1}		3580.196[c,f]
a_0/cm^{-1}		325.0[c]
a_1		1.636[c]
a_2		1.990[c]

[a]The uncertainties represent 95% confidence intervals. Parameters given without uncertainties were held fixed. [b]This parameter was adjusted by hand. Its large value in combination with the small value of B_Π is a consequence of the weakly bound nature of the $^2\Pi_u$ state. [c]This parameter was kept constant during the fit. [d]Values from ref 52. [e]Determined from $R_{e,\Lambda}$ and $D_{e,\Lambda}$ using eqs 7 and 8. [f]Value from ref 60.

The results of the least-squares fits for Ar_2^+ and Kr_2^+ are presented in the next two subsections and serve as a basis for the discussion of the effects of the R dependence of the spin−orbit-coupling constant on the potential functions and energy levels of Ar_2^+ and Kr_2^+.

A. Ar_2^+. A total of 66 (26) experimental level positions were used in the fit of the u (g) states of Ar_2^+, 52 (16) for $^{40}Ar_2^+$, and 14 (10) for $^{36}Ar_2^+$, as described in section IV (also see Tables 7−11). The results of the fits are summarized in Table 3, which contains the numerical values of all parameters needed to compute the potential energy functions of the six low-lying electronic states of Ar_2^+ using eq 1 and Table 1, including the parameters that were kept constant in the fitting procedure.

The RMS value of the fits of the u and g states are both slightly less than 1, which indicates that the potential energy functions describe the experimental data well. Table 3 also contains the dissociation energy and the equilibrium internuclear distances of the fictive $^2\Sigma^+$ and $^2\Pi$ states. As expected from earlier work and also from simple considerations based on linear combinations of the atomic p valence orbitals, only the $^2\Sigma_u^+$ state is strongly bound, and the $^2\Sigma_g^+$ state is repulsive at short-range.

The equilibrium internuclear separations and dissociation energies of the six low-lying states of Ar_2^+ are given in Table 4,

Table 6. Dissociation Energies D_e and Equilibrium Internuclear Distances R_e of the Lowest *ungerade* Electronic States of Kr_2^+ Determined from the Potential Energy Curves Displayed in Figure 7

	I(1/2u)	I(3/2u)	II(1/2u)	reference
D_e/cm^{-1}	9361.5	383.0	1099.8	this work
	9360.1	381.9	1091.3	52
	9492	260	966	29
	9361.2 ± 2.8	382.8 ± 1.9	1099.9 ± 2.1	43
R_e/Å	2.692	4.154	3.771	this work
	2.697	4.110	3.732	52
	2.6945	4.2132	3.7211	29
		4.11 ± 0.04	3.78 ± 0.04	43

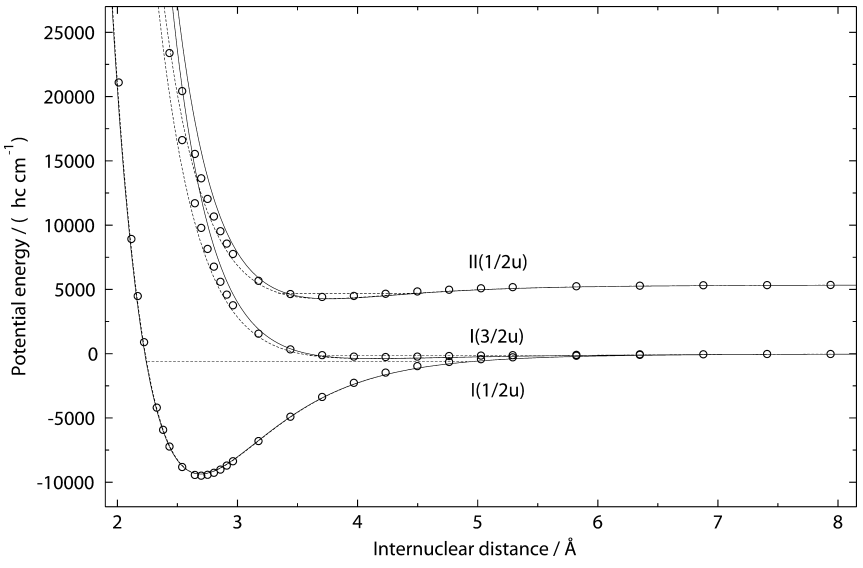

Figure 7. Comparison of the potential energy functions of the I(1/2u), I(3/2u), and II(1/2u) states of Kr_2^+ derived in this work (full line), in ref 52 (dashed line) and in ref 29 (circles). The dashed horizontal lines indicate for each state the positions of the highest observed vibrational level.

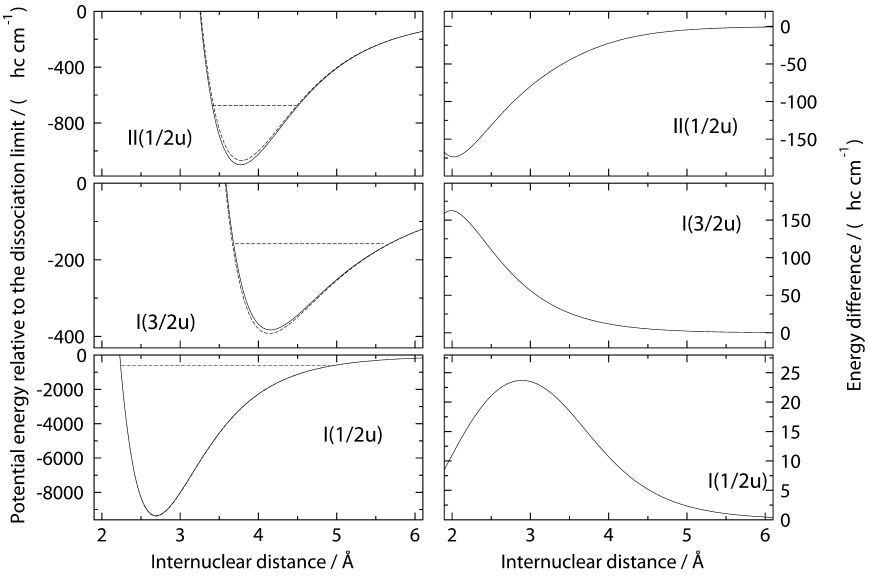

Figure 8. Left panels: Potential energy functions of the I(1/2*u*) (bottom), I(3/2*u*) (middle), and II(1/2*u*) (top) states of Kr_2^+ calculated with *R*-dependent $a_u(R)$ (full lines) and *R*-independent $a = a_{Kr^+}$ (dashed lines) using the same Σ and Π potential energy curves (parameter set for the *u* states in Table 5). The dashed horizontal lines indicate for each state the positions of the highest observed vibrational level. Right panels: Energy difference of the two curves displayed in the left panels for the I(1/2*u*) (bottom), I(3/2*u*) (middle), and II(1/2*u*) (top) states of Kr_2^+.

Table 7. Measured Positions ($\tilde{\nu}_{obs}$) and Differences between Measured and Calculated Positions ($\Delta\tilde{\nu} = \tilde{\nu}_{calc} - \tilde{\nu}_{obs}$) of the Vibrational Levels of the I(1/2u) State of Ar_2^+ [a]

	$^{40}Ar_2^+$		$^{36}Ar_2^+$			$^{40}Ar_2^+$		$^{36}Ar_2^+$	
v^+	$\tilde{\nu}_{obs}$	$\Delta\tilde{\nu}$ [b]	$\tilde{\nu}_{obs}$	$\Delta\tilde{\nu}$ [b]	v^+	$\tilde{\nu}_{obs}$	$\Delta\tilde{\nu}$ [b]	$\tilde{\nu}_{obs}$	$\Delta\tilde{\nu}$ [b]
0		116585.9		116593.3	26	123115.9(30)	−0.5		123391.1
1		116889.5		116913.1	27	123307.9(30)	−1.8		123588.0
2		117188.9		117228.3	28	123496.6(30)	−1.9		123779.9
3	117488.5(30)	4.2		117538.9	29	123681.9(30)	−0.9		123966.8
4		117775.5		117845.0	30	123862.2(30)	−0.5		124148.7
5	118066.1(30)	3.5		118146.4	31	124037.2(30)	−0.9		124325.6
6	118347.8(30)	2.3		118443.2	32	124207.9(30)	−1.0		124497.4
7	118626.3(30)	2.1		118735.3	33	124373.7(30)	−1.6		124664.1
8	118901.4(30)	2.6		119022.8	34	124535.5(30)	−1.5		124825.6
9	119172.3(30)	3.1		119305.7	35	124693.1(6)	−1.0		124981.9
10	119437.4(22)	2.0		119583.9	36	124845.7(7)	−0.9		125133.1
11		119697.5		119857.5	37	124993.9(6)	−0.5		125278.9
12	119955.7(30)	0.4		120126.3	38	125137.1(6)	−0.5	125418.9(7)	−0.6
13	120209.5(30)	0.7		120390.5	39	125275.2(6)	−0.7	125554.4(7)	−0.2
14	120458.8(30)	0.6		120650.0	40	125409.3(7)	−0.2	125684.4(7)	−0.01
15	120703.7(30)	0.4		120904.7	41	125538.6(7)	0.3	125807.8(7)	−0.9
16	120944.5(22)	0.3		121154.7	42	125662.1(6)	−0.1	125927.3(7)	−0.2
17	121180.3(30)	−0.5		121400.0	43	125781.5(7)	0.3	126041.0(7)	0.2
18	121413.2(30)	0.04		121640.5	44	125896.8(7)	1.5	126148.6(7)	0.2
19	121640.5(30)	−0.7		121876.2	45	126004.6(7)	0.3	126250.7(7)	0.3
20	121863.5(30)	−1.5	122106.3(30)	−0.9	46	126108.6(7)	0.2	126347.2(7)	0.6
21	122083.4(21)	−1.0	122332.0(30)	−1.3	47	126207.9(7)	0.6		126437.2
22	122299.2(30)	−0.3		122554.6	48	126301.6(7)	0.4		126522.0
23	122508.6(30)	−1.7		122771.1	49	126391.1(7)	1.2		126601.1
24	122715.5(30)	−1.2		122982.6	50	126474.3(7)	0.9		126674.4
25	122918.0(30)	−0.8		123189.4	DL[c]		127194.282		127193.492

[a] All positions are in cm^{-1} and are given relative to the position of the rovibronic ground state of the corresponding isotopomer of Ar_2^+. The experimental positions include the field-induced shift of the ionization thresholds. Experimental data from ref 74. [b] Whenever no experimental data could be determined, the calculated values were listed. [c] DL denotes the position of the $Ar(^1S_0) + Ar^+(^2P_{3/2})$ dissociation limit.

where they are compared with the results of selected high-level *ab initio* calculations[24,29] (both relying on the assumption of an *R*-independent spin−orbit-coupling constant $a = a_{Ar^+}$).

They are also compared with the values obtained in ref 49, which relied on the same experimental data set and the same procedure as the present work, except that the spin−orbit-coupling

Table 8. Measured Positions ($\tilde{\nu}_{obs}$) and Differences between Measured and Calculated Positions ($\Delta\tilde{\nu} = \tilde{\nu}_{calc} - \tilde{\nu}_{obs}$) of the Vibrational Levels of the I(3/2u) State of Ar_2^+ [a]

	$^{40}Ar_2^+$		$^{36}Ar_2^+$	
v^+	$\tilde{\nu}_{obs}$	$\Delta\tilde{\nu}$ [b]	$\tilde{\nu}_{obs}$	$\Delta\tilde{\nu}$ [b]
0	126882.5(15)	−1.2	126882.8(6)	−1.1
1	126919.9(20)	−0.8	126922.8(6)	0.04
2	126954.0(25)	−0.7	126957.9(7)	−0.3
DL[c]		127194.282		127193.492

[a]All positions are in cm^{-1} and are given relative to the position of the rovibronic ground state of the corresponding isotopomer of Ar_2^+. The experimental positions include the field-induced shift of the ionization thresholds. Experimental data from ref 74. [b]Whenever no experimental data could be determined, the calculated values were listed. [c]DL denotes the position of the $Ar(^1S_0) + Ar^+(^2P_{3/2})$ dissociation limit.

Table 9. Measured Positions ($\tilde{\nu}_{obs}$) and Differences between Measured and Calculated Positions ($\Delta\tilde{\nu} = \tilde{\nu}_{calc} - \tilde{\nu}_{obs}$) of the Vibrational Levels of the II(1/2u) State of Ar_2^+ [a]

	$^{40}Ar_2^+$		$^{36}Ar_2^+$	
v^+	$\tilde{\nu}_{obs}$	$\Delta\tilde{\nu}$ [b]	$\tilde{\nu}_{obs}$	$\Delta\tilde{\nu}$ [b]
0	128001.0(7)	−0.8		128002.5
1	128057.0(7)	0.3		128060.3
2	128110.4(7)	1.1		128115.4
DL[c]		128625.865		128625.075

[a]All positions are in cm^{-1} and are given relative to the position of the rovibronic ground state of the corresponding isotopomer of Ar_2^+. The experimental positions include the field-induced shift of the ionization thresholds. Experimental data from ref 74. [b]Whenever no experimental data could be determined, the calculated values were listed. [c]DL denotes the position of the $Ar(^1S_0) + Ar^+(^2P_{1/2})$ dissociation limit.

Table 10. Measured Positions ($\tilde{\nu}_{obs}$) and Differences between Measured and Calculated Positions ($\Delta\tilde{\nu} = \tilde{\nu}_{calc} - \tilde{\nu}_{obs}$) of the Vibrational Levels of the I(1/2g) State of Ar_2^+ [a]

	$^{40}Ar_2^+$		$^{36}Ar_2^+$	
v^+	$\tilde{\nu}_{obs}$	$\Delta\tilde{\nu}$ [b]	$\tilde{\nu}_{obs}$	$\Delta\tilde{\nu}$ [b]
0		126589.9[c]		126592.0[c]
1	126692.5(30)[c]	−2.5		126702.4[c]
2	126792.8(15)[c]	−0.8		126805.6[c]
3	126884.0(15)[c]	−1.1	126899.4(7)[c]	−1.3
4	126968.9(15)[c]	0.3	126986.8(7)[c]	0.1
5	127044.4(20)[c]	2.1		127061.0[c]
6		127086.8[c]		127086.4[c]
7		127100.4[d]		127101.1[d]
8		127102.2[e]		127112.8[e]
DL[f]		127194.282		127193.492

[a]All positions are in cm^{-1} and are given relative to the position of the rovibronic ground state of the corresponding isotopomer of Ar_2^+. The experimental positions include the field-induced shift of the ionization thresholds. Experimental data from ref 74. [b]Whenever no experimental data could be determined, the calculated values were listed. [c]Corresponding vibrational wave function is mostly located in the inner well of the potential energy curve. [d]Corresponding vibrational wave function is mostly located in the outer well of the potential energy curve. [e]Corresponding vibrational wave function is located in the inner and the outer wells of the potential energy curve. [f]DL denotes the position of the $Ar(^1S_0) + Ar^+(^2P_{3/2})$ dissociation limit.

constant was assumed to be independent of R. The similarity of the results obtained from these two fits suggests that the effects

Table 11. Measured Positions ($\tilde{\nu}_{obs}$) and Differences between Measured and Calculated Positions ($\Delta\tilde{\nu} = \tilde{\nu}_{calc} - \tilde{\nu}_{obs}$) of the Vibrational Levels of the I(3/2g) State of Ar_2^+ [a]

	$^{40}Ar_2^+$		$^{36}Ar_2^+$	
v^+	$\tilde{\nu}_{obs}$	$\Delta\tilde{\nu}$ [b]	$\tilde{\nu}_{obs}$	$\Delta\tilde{\nu}$ [b]
0	125685.0(15)	0.2	125687.5(6)	0.4
1	125797.8(20)	−0.3	125806.9(6)	0.6
2	125905.7(15)	−0.9	125920.1(7)	−0.1
3	126009.0(15)	−1.3	126028.9(6)	0.3
4	126107.4(25)	−1.7	126132.0(7)	0.4
5	126202.7(15)	−0.4	126229.6(6)	0.3
6	126292.4(15)	0.1	126321.4(7)	−0.3
7	126376.5(15)	−0.2	126408.9(7)	0.2
8	126455.7(15)	−0.6		126490.4
9	126531.0(30)	−0.1		126566.9
10	126604.0(30)	2.8		126638.1
DL[c]		127194.282		127193.492

[a]All positions are in cm^{-1} and are given relative to the position of the rovibronic ground state of the corresponding isotopomer of Ar_2^+. The experimental positions include the field-induced shift of the ionization thresholds. Experimental data from ref 74. [b]Whenever no experimental data could be determined, the calculated values were listed. [c]DL denotes the position of the $Ar(^1S_0) + Ar^+(^2P_{3/2})$ dissociation limit.

of the R dependence of a are weak. Indeed, inspection of the potential energy functions derived from both fits and displayed in Figures 4 and 5 only reveals significant deviations at short internuclear distances, where the potential energy functions are not constrained by the experimental observations. However, the comparison does not enable one to precisely quantify the effects of the R dependence on the potential functions because these effects are likely to be compensated by other fit parameters.

To quantify the consequences of approximating the spin−orbit-coupling constant to the atomic value a_{Ar^+}, two sets of calculations were performed relying on the same potential energy functions $V_\Sigma(R)$ and $V_\Pi(R)$, as given in Table 3, one using the R-dependent functions $a_{g,u}(R)$ presented in section III, the other using $a_{g,u} = a_{Ar^+}$. The results of these calculations for the u states are depicted in Figure 6, which compares the potential energy functions on the left-hand side and shows their difference on the right-hand side. The dashed horizontal lines in the figure indicate the highest vibrational levels observed for each electronic state and enable one to directly see the range of internuclear distances covered by the experimental data, i.e., 2−4.5 Å for the I(1/2u) state, 3.5−4.5 Å for the I(3/2u) state, and 3.3−4.2 Å for the II(1/2u) state.

Figure 6 shows that the neglect of the R dependence of a has an extremely small effect on the potential energy functions of I(1/2u), the differences being less than 2 cm^{-1} over the entire range of internuclear distances. The differences are larger for the I(3/2u) and II(1/2u) states, particular below 3 Å, where they reach values up to 45 cm^{-1}, but they remain very small (less than 5 cm^{-1}) over the range of internuclear separation relevant for the analysis of the photoelectron spectroscopic data. The deviations are of the same magnitude but opposite sign for the I(3/2u) and II(1/2u) states. This behavior indicates that the dominant effect originates from the diagonal (first-order) contribution of the spin−orbit operator in Table 1. The value of the spin−orbit-coupling functions $a_u(R)$ is less than a_{Ar^+}, so that the splitting between the two components of the Π_u state is slightly reduced. This effect raises (lowers) the potential energy of the I(3/2u) (II(1/2u)) state in the

dx.doi.org/10.1021/ct300078m | J. Chem. Theory Comput. 2012, 8, 3671−3685

Table 12. Measured Positions ($\tilde{\nu}_{obs}$) and Differences between Measured and Calculated Positions ($\Delta\tilde{\nu} = \tilde{\nu}_{calc} - \tilde{\nu}_{obs}$) of the Vibrational Levels of the I(1/2u) State of Kr_2^+ [a]

	$^{84}Kr_2^+$		$^{84}Kr-^{86}Kr^+$			$^{84}Kr_2^+$		$^{84}Kr-^{86}Kr^+$	
v^+	$\tilde{\nu}_{obs}$	$\Delta\tilde{\nu}$ [b]	$\tilde{\nu}_{obs}$	$\Delta\tilde{\nu}$ [b]	v^+	$\tilde{\nu}_{obs}$	$\Delta\tilde{\nu}$ [b]	$\tilde{\nu}_{obs}$	$\Delta\tilde{\nu}$ [b]
0	103773.6(6)	0.5		103772.6	38	109547.5(10)	−2.4		109523.7
1	103956.6(28)	−1.9		103956.9	39	109663.0(15)	−2.2		109638.8
2		104142.2		104139.5	40	109776.1(16)	−2.5		109752.0
3		104324.1		104320.4	41	109888.4(22)	−1.7		109863.3
4		104504.3		104499.6	42	109997.7(20)	−1.8		109972.5
5	104684.4(5)	1.7		104677.0	43	110105.2(19)	−1.8		110079.9
6	104860.6(15)	1.2		104852.7	44	110211.3(23)	−1.2		110185.3
7		105034.2		105026.6	45	110314.2(19)	−1.8		110288.7
8		105207.4		105198.8	46	110416.0(15)	−1.5		110390.1
9		105378.7		105369.3	47	110515.3(23)	−1.6		110489.6
10		105548.3		105537.9	48	110613.4(11)	−1.0		110587.1
11		105716.0		105704.8	49	110708.7(23)	−1.2		110682.6
12		105882.0		105870.0	50	110802.9(25)	−0.5		110776.1
13		106046.2		106033.4	51	110894.2(16)	−0.7		110867.6
14		106208.6		106195.0	52	110983.9(11)	−0.4		110957.1
15	106369.4(7)	0.2		106354.8	53	111071.7(8)	−0.01		111044.6
16	106528.3(12)	0.3		106512.8	54		111157.1		111130.2
17	106685.2(20)	0.3		106669.0	55	111240.8(16)	0.3		111213.7
18	106838.2(28)	−1.9		106823.4	56	111322.7(19)	0.9	111295.7(21)	0.5
19		106993.4		106976.0	57	111401.5(15)	0.4	111375.4(9)	0.6
20	107143.5(17)	−1.3		107126.8	58	111479.7(9)	1.3	111453.6(13)	1.3
21		107294.4		107275.8	59	111555.1(19)	1.4	111529.1(30)	1.3
22	107440.1(20)	−2.1		107422.9	60	111628.9(13)	2.0	111603.2(23)	1.9
23		107588.1		107568.2	61		111698.2		111672.8
24	107730.9(16)	−1.3		107711.7	62	111769.2(15)	1.8		111742.4
25	107872.8(22)	−1.6		107853.3	63	111837.2(19)	2.7		111809.9
26	108012.8(12)	−1.9		107993.1	64	111902.2(14)	2.5		111875.4
27	108150.7(26)	−2.4		108131.0	65	111965.6(13)	2.8		111938.9
28	108288.3(10)	−1.3		108267.1	66	112027.0(12)	3.0		112000.5
29	108422.7(16)	−1.6		108401.3	67	112086.8(29)	3.7		112060.0
30		108557.0		108533.6	68		112140.2		112117.6
31		108687.9		108664.0	69	112199.0(11)	3.6		112173.2
32	108814.7(12)	−2.1		108792.5	70		112248.5		112226.9
33	108942.5(17)	−1.3		108919.2	71		112299.7		112278.6
34		109068.9		109043.9	72		112348.9		112328.3
35	109190.0(14)	−2.1		109166.7	73	112399.8(15)	3.7		112376.1
36	109310.9(13)	−2.4		109287.6	74	112445.5(11)	4.1		112422.0
37	109430.0(16)	−2.6		109406.6	DL[c]		113041.23		113041.23

[a] All positions are in cm^{-1} and are given relative to the position of the rovibronic ground state of the corresponding isotopomer of Kr_2^+. The experimental positions include the field-induced shift of the ionization thresholds. Experimental data from ref 52. [b] Whenever no experimental data could be determined, the calculated values were listed. [c] DL denotes the position of the $Kr(^1S_0) + Kr^+(^2P_{3/2})$ dissociation limit.

calculations performed with the *R*-dependent spin−orbit-coupling constant. The very small shift of the I(1/2*u*) potential energy curves is caused by the off-diagonal (second-order) spin−orbit-coupling matrix elements in Table 1 and can be explained by the fact that the spin−orbit-coupling constant is much smaller than the difference between the Σ_u^+ and Π_u potential functions in the range of *R* values where $a_u(R)$ significantly deviates from the asymptotic value a_{Ar^+}. The difference of the binding energies of the Σ_u^+ and Π_u states in the vicinity of the potential minima is indeed more than 10 times larger than the spin−orbit-coupling constant.

Similar conclusions apply to the *gerade* states of Ar_2^+ if one takes into account the different energetic ordering of the Π and Σ states ($^2\Sigma_g^+$ lies above $^2\Pi_g$), the smaller difference in the binding energies of these to states (see Table 3), and the fact that $a_g(R)$ is larger than a_{Ar^+} (see Figure 2). Consequently, the I(3/2*g*) [II(1/2*g*)] curve calculated with $a_g(R)$ lies below [above] that calculated with a_{Ar^+}. The two Ω = 1/2 states are more strongly mixed, so that the shifts of the I(3/2*g*) and II(1/2*g*) states are less symmetric than is the case for the I(3/2*u*) and II(1/2*u*) states.

B. Kr_2^+. A total of 91 experimental level positions were used in the fit of the *ungerade* states of Kr_2^+, 72 for $^{84}Kr_2^+$, and 19 for $^{86}Kr^{84}Kr^+$, as described in section IV (see also Tables 12−14). The high-resolution photoelectron-spectroscopic data on the *gerade* states are limited to the I(3/2*g*) state and are insufficient for a global treatment of these states based on the spin−orbit interaction matrix presented in Table 1. This subsection thus focuses on the least-squares fit of the *ungerade* states I(1/2*u*), I(3/2*u*), and II(1/2*u*). The same experimental data set was used in the derivation of the potential energy curves of these states under the assumption of an *R*-independent spin−orbit-coupling constant.[52]

Table 13. Measured Positions ($\tilde{\nu}_{obs}$) and Differences between Measured and Calculated Positions ($\Delta\tilde{\nu} = \tilde{\nu}_{calc} - \tilde{\nu}_{obs}$) of the Vibrational Levels of the I(3/2u) State of Kr_2^+ [a]

	$^{84}Kr_2^+$		$^{84}Kr-^{86}Kr^+$	
v^+	$\tilde{\nu}_{obs}$	$\Delta\tilde{\nu}$ [b]	$\tilde{\nu}_{obs}$	$\Delta\tilde{\nu}$ [b]
0	112672.4(2)	0.08	112672.4(4)	0.2
1	112699.6(3)	0.2	112699.4(6)	0.2
2	112725.0(3)	−0.2	112724.9(6)	0.1
3	112749.4(3)	0.08	112748.9(7)	−0.1
4	112772.2(4)	−0.3	112771.6(5)	−0.3
5	112793.8(3)	−0.3	112793.3(10)	−0.1
6	112814.3(7)	−0.2	112813.1(14)	−0.6
7	112833.2(9)	−0.4		112832.8
8	112851.2(4)	−0.3		112850.6
9	112867.8(7)	−0.4		112867.3
10	112883.1(7)	−0.7		112882.9
DL[c]		113041.23		113041.23

[a]All positions are in cm^{-1} and are given relative to the position of the rovibronic ground state of the corresponding isotopomer of Kr_2^+. The experimental positions include the field-induced shift of the ionization thresholds. Experimental data from ref 52. [b]Whenever no experimental data could be determined, the calculated values were listed. [c]DL denotes the position of the $Kr(^1S_0) + Kr^+(^2P_{3/2})$ dissociation limit.

Table 14. Measured Positions ($\tilde{\nu}_{obs}$) and Differences between Measured and Calculated Positions ($\Delta\tilde{\nu} = \tilde{\nu}_{calc} - \tilde{\nu}_{obs}$) of the Vibrational Levels of the II(1/2u) State of Kr_2^+ [a]

	$^{84}Kr_2^+$		$^{84}Kr-^{86}Kr^+$	
v^+	$\tilde{\nu}_{obs}$	$\Delta\tilde{\nu}$ [b]	$\tilde{\nu}_{obs}$	$\Delta\tilde{\nu}$ [b]
0	117339.3(10)	−0.3		117339.5
1	117394.3(11)	−0.1		117393.9
2	117447.6(4)	−0.06		117446.9
3	117499.5(5)	0.09	117498.4(10)	0.03
4	117549.8(4)	0.1	117548.4(7)	0.05
5	117598.7(5)	0.3	117597.0(6)	0.2
6	117645.8(5)	0.2	117644.2(9)	0.4
7	117691.9(7)	0.7	117689.9(12)	0.7
8	117736.1(13)	0.8	117734.1(12)	0.9
9		117777.9	117776.8(22)	1.2
DL[c]		118411.53		118411.53

[a]All positions are in cm^{-1} and are given relative to the position of the rovibronic ground state of the corresponding isotopomer of Kr_2^+. The experimental positions include the field-induced shift of the ionization thresholds. Experimental data from ref 52. [b]Whenever no experimental data could be determined, the calculated values were listed. [c]DL denotes the position of the $Kr(^1S_0) + Kr^+(^2P_{1/2})$ dissociation limit.

The optimal fit parameters are listed in Table 5. Only eight of these were varied in the fitting procedure, as explained in section II, the remaining ones being kept at the literature values indicated in the table. The RMS value of the fit was 1.2, about half the RMS value of 2.2 obtained in the analysis based on the assumption of an *R*-independent spin−orbit-coupling constant.[52] The dissociation energies of the fictive $^2\Sigma_u^+$ and $^2\Pi_u$ states (10922.5 cm^{-1} and 392 cm^{-1}, respectively) are similar to the values found for Ar_2^+, as expected.

The potential energy functions of the three low-lying *u* states of Kr_2^+ are displayed in Figure 7. Their dissociation energies and equilibrium internuclear distances are compared with the results of earlier investigations in Table 6. Comparing the present results with those obtained assuming an *R*-independent spin−orbit-coupling constant in ref 52 leads to the conclusion that the main discrepancy affects the II(1/2*u*) state for which a systematic trend in the residuals from +7.6 cm^{-1} at $v = 0$ to −5.7 cm^{-1} at $v = 8$ was noted in ref 52 (see Table 3 of this reference). The present analysis is free of this trend and yields a dissociation energy of 1099.8 cm^{-1} for the II(1/2*u*) state, in better agreement with the value of 1099.9 ± 2.1 cm^{-1} determined experimentally in ref 43. This observation, combined with the improved RMS value, indicates that the consideration of the *R* dependence of *a* leads to potential curves of higher accuracy, particularly for the II(1/2*u*) state.

To quantify the effects of the assumption of an *R*-independent spin−orbit-coupling constant used in previous work on the low-lying electronic states of Kr_2^+, the same procedure was used as described in the previous subsection for Ar_2^+. The results are presented in Figure 8, which displays, on the left-hand side, the two sets of curves calculated with the same potential functions V_Σ and V_Π (with parameters as given in Table 5) but using the function $a_u(R)$ determined in section III in one case (full line) and a_{Kr^+} in the other (dashed lines). The differences between these two set of curves are plotted on the right-hand side of the figure.

The overall trends of the differences are similar to those observed for Ar_2^+ in Figure 6, but the deviations are 4−5 times larger. While in the case of Ar_2^+ the deviations of less than 5 cm^{-1} are on the same order of magnitude as the experimental uncertainties, they are larger in the case of Kr_2^+, which makes the effects of the *R*-dependence of *a* detectable. Over the range of *R* values for which experimental data are available (indicated by the dashed horizontal lines in Figure 8), i.e., 2.2−5 Å for the I(1/2*u*) state, 3.6−5.6 Å for the I(3/2*u*) state, and 3.4−4.5 Å for the II(1/2*u*) state, the deviations vary from 5 to 20 cm^{-1} for the I(1/2*u*) state, 2 to 20 cm^{-1} for the I(3/2*u*) state, and 5 to 60 cm^{-1} for the II(1/2*u*) state. The particularly large deviations predicted for the II(1/2*u*) state nicely explain why the consideration of the *R* dependence of the spin−orbit-coupling constant is necessary to satisfactorily account for the experimental data obtained for this state.

The larger effects of the *R* dependence of the spin−orbit coupling constant in Kr_2^+ compared to Ar_2^+ result from three simultaneous effects: (i) The absolute value of the spin−orbit-coupling constant increases from ∼950 cm^{-1} in Ar_2^+ to ∼3500 cm^{-1} in Kr_2^+, while (ii) the difference in binding energies of the Σ and Π states is roughly the same for both ions (i.e., about 10 000 cm^{-1}), and (iii) the absolute value of the deviations between $a(R)$ and a_{Rg^+} are three times larger in Kr_2^+ (up to 300 cm^{-1}) than in Ar_2^+ (up to 100 cm^{-1}). Effect iii directly influences the potential energies of the I(3/2*u*), II(1/2*u*), I(3/2*g*), and I(1/2*g*) states via the diagonal (first-order) elements of the spin−orbit-coupling matrix, and the combination of i and ii leads to a larger mixing of the two Ω = 1/2 states induced by the off-diagonal elements of the spin−orbit-coupling matrix in the case of Kr_2^+ than in the case of Ar_2^+. The mixing of the Ω = 1/2 levels and the effects of the *R* dependence of the spin−orbit-coupling constant are expected to be even larger on the *gerade* states of Kr_2^+ because the difference in binding energies of the $^2\Pi_g$ and $^2\Sigma_g^+$ states is smaller in the range of internuclear distances where $a_g(R)$ strongly deviates from a_{Kr^+}. The *R* dependence of a_g is thus expected to result in a destabilization of the II(1/2*g*) state and may be the main reason why this state, and also the II(1/2*g*) of Xe_2^+, have not been observed yet in high-resolution photoelectron spectroscopic experiments.

dx.doi.org/10.1021/ct300078m | J. Chem. Theory Comput. 2012, 8, 3671−3685

VI. CONCLUSIONS

The spin−orbit interaction strongly influences the structural and spectral properties of the homonuclear rare-gas dimer ions (Rg_2^+, Rg = Ne, Ar, Kr, Xe). Until recently, the spin−orbit-coupling constants used in the derivation of the potential energy functions of the six low-lying electronic states of these molecular ions were assumed to be independent of the internuclear separation and equal to their "atomic" value a_{Rg^+}. Together with our previous investigation of the potential energy functions of Xe_2^+, the investigation of the potential energy functions of the low-lying electronic states of Ar_2^+ and Kr_2^+ presented in this article provides a quantification of the R dependence of the spin−orbit constant in these systems and a systematic examination of the consequences associated with its neglect.

The spin−orbit-coupling constant maximally deviates from the atomic value by up to about 10%, and the deviations have opposite signs for the electronic states of *gerade* and *ungerade* symmetry. The R dependences can be accurately represented by analytical functions, a Morse-type function for the *ungerade* states, and an exponentially decaying function for the *gerade* states. The effects of the R dependence on the potential energy functions are almost entirely negligible for Ar_2^+ (and by inference also for Ne_2^+). They manifest themselves as shifts of the potential energy functions and spin−rovibronic energy levels of at most a few cm^{-1} and are expected to only be observable in very high-resolution spectroscopic measurements. In Kr_2^+ and Xe_2^+, the R dependence leads to more pronounced effects and needs to be considered in the analysis of high-resolution photoelectron spectra and in the description of the potential energy functions of the low-lying electronic states.

The increasingly important impact of the R dependence of the spin−orbit-coupling constant on the properties of the *ungerade* states from Ne_2^+ to Xe_2^+ can be explained by the fact that the difference in binding energies between the $^2\Pi_u$ and $^2\Sigma_u^+$ states that are coupled by the spin−orbit interaction slowly decreases, from about 12 000 cm^{-1} in Ne_2^+ [29] to about 9000 cm^{-1} in Xe_2^+,[56] whereas the atomic spin−orbit-coupling constant rapidly increases from about 520.282 cm^{-1} in Ne_2^+ [59] to 7024.617 cm^{-1} in Xe_2^+.[73]

The effects of the spin−orbit interaction on the $^2\Sigma_u^+$ state originate from the off-diagonal element of the spin−orbit interaction matrix, which couples it to the upper $^2\Pi_u$ component of the $^2\Pi$ states. Because the $^2\Sigma_u^+$ state lies below the $^2\Pi_u$ state, the interaction shifts the potential energy function of the former state toward lower energies and that of the latter toward higher energies. The R-dependent spin−orbit-coupling constants of the u states are reduced compared to the atomic value, so that assuming the spin−orbit constant to be independent of R leads to an overestimation of the potential energies. The range of internuclear distances where the spin−orbit-coupling constant significantly deviates from the atomic value corresponds closely to the region where the $^2\Sigma_u^+$ state is strongly bound. In this region, the mixing between the $^2\Sigma_u^+$ and the $^2\Pi_{1/2u}$ states is very weak in Ne_2^+ and Ar_2^+, because the spin−orbit constant is too small to induce a significant mixing between these two states. The effect of the R dependence of a_u is thus negligible in these two molecular ions. In Kr_2^+ and Xe_2^+, the spin−orbit-coupling constant is larger, and the level shifts resulting from the R dependence of the spin−orbit-coupling constant (or its neglect) are on the order of about 20 cm^{-1} for the $I(1/2u)$ state of Kr_2^+ (see Figure 6) and 50 cm^{-1} for the $I(1/2u)$ state of Xe_2^+ (see Figure 7d of ref 56) and thus easily observable spectroscopically.

The effects of the R dependence of the spin−orbit-coupling constant on the $I(3/2u)$ state originates from the diagonal (first-order) contribution $(-a(R)/2)$ of the Hamiltonian. The potential energy shifts resulting from the R dependence of the spin−orbit-coupling constant (or its neglect) thus closely track the value $|(a(R) - a_{Rg^+})|/2$. These shifts are in general much larger than the shifts arising from the off-diagonal coupling.

The effects of the R dependence of the spin−orbit-coupling constant of the $II(1/2u)$ state are an additive combination of the two effects described above for the $I(1/2u)$ and $I(3/2u)$ states. They are thus largest for this state although strongly dominated by the diagonal contribution of the spin−orbit-coupling matrix. Consequently, the potential energy shifts of the $I(3/2u)$ and $II(1/2u)$ states resulting from a neglect of the R dependence of the spin−orbit constant are of similar magnitude but of opposite signs (see upper two panels on the right-hand side of Figures 6 and 8 and of Figure 7 of ref 52).

The effect of the R dependence of the spin−orbit-coupling constant on the *gerade* electronic states can be described by the same arguments, taking into account the facts that (i) the function $a(R)$ is larger than a_{Rg^+}, (ii) the $^2\Sigma_g^+$ state is less strongly bound than the $^2\Pi_g$ state, and (iii) the diagonal contribution of the spin−orbit component shifts the upper spin−orbit component of the $^2\Pi_g$ state toward the $^2\Sigma_g^+$ state. While the effects of the R dependence of the spin−orbit-coupling constants are still almost negligible in Ne_2^+ and Ar_2^+ for the same reasons as for the *ungerade* states, the shifts resulting from the R dependence (or its neglect) are expected to be of opposite signs, and the shifts arising from the off-diagonal contribution to be more pronounced, than for the *ungerade* states.

The experimental data available on the $I(1/2\ g)$ and $II(1/2\ g)$ states of Ar_2^+ and Kr_2^+ are still very incomplete as a result of the repulsive nature of these states at short internuclear distances. In the future, one may be able to obtain information on the repulsive part of the potential energy functions of these states by imaging techniques, as was recently demonstrated for Xe_2^+ in ref 8.

APPENDIX

Tables 7−14, which have been presented earlier and mentioned throughout the paper, provide a complete list of the positions of the vibrational levels of Ar_2^+ and Kr_2^+ measured experimentally by pulsed-field ionization zero-kinetic-energy photoelectron spectroscopy. The tables also contain the experimental uncertainties used in the least-squares fits and the deviations between experimental positions and those calculated with the new sets of potential energy functions described in this article. Further details specific to the different tables are provided in the respective table captions.

AUTHOR INFORMATION

Corresponding Author

*E-mail: markus.reiher@phys.chem.ethz.ch, merkt@phys.chem.ethz.ch.

Notes

The authors declare no competing financial interest.

ACKNOWLEDGMENTS

We thank Dr. R. A. Dressler for discussions and encouragement to perform the investigations described in this article. We take

this article as opportunity to thank Prof. Wilfred F. van Gunsteren for his stimulating influence and fruitful scientific exchanges over many years. This work is supported financially by the Swiss National Science Foundation under Projects Nr. 200020-132542/1 (M.R.) and Nr. 200020-135342 (F.M.).

REFERENCES

(1) Mulliken, R. S. *J. Chem. Phys.* **1970**, *52*, 5170−5180.
(2) Miller, J. S.; Pullins, S. H.; Levandier, D. J.; hui Chiu, Y.; Dressler, R. A. *J. Appl. Phys.* **2002**, *91*, 984−991.
(3) Boyd, I. D.; Dressler, R. A. *J. Appl. Phys.* **2002**, *92*, 1764−1774.
(4) Rhodes, Ch. K. *Excimer Lasers*, 2nd ed.; Springer: Berlin, 1984; Vol. 30 of Topics in Applied Physics.
(5) Eden, J. G. *IEEE J. Sel. Top. Quantum Electron.* **2000**, *6*, 1051−1060.
(6) Samson, J. A. R.; Ederer, D. L. *Vacuum Ultraviolet Spectroscopy*; Academic Press: San Diego, 2000.
(7) Ewing, J. J. *IEEE J. Sel. Top. Quantum Electron.* **2000**, *6*, 1061−1071.
(8) Shubert, V. A.; Pratt, S. T. *J. Chem. Phys.* **2011**, *134*, 044315.
(9) Hopkins, W. S.; Mackenzie, S. R. *J. Chem. Phys.* **2011**, *135*, 081104.
(10) Piticco, L.; Schäfer, M.; Merkt, F. *J. Chem. Phys.* **2012**, *136*, 074304.
(11) Kalus, R.; Paidarová, I.; Hrivňák, D.; Paška, P.; Gadéa, F. X. *Chem. Phys.* **2003**, *294*, 141−153.
(12) Kalus, R.; Paidarová, I.; Hrivňák, D.; Gadéa, F. X. *Chem. Phys.* **2004**, *298*, 155−166.
(13) Poterya, V.; Fárník, M.; Buck, U.; Bonhommeau, D.; Halberstadt, N. *Int. J. Mass Spectrom.* **2009**, *280*, 78−84.
(14) Gilbert, T. L.; Wahl, A. C. *J. Chem. Phys.* **1971**, *55*, 5247−5261.
(15) Michels, H. H.; Hobbs, R. H.; Wright, L. A. *J. Chem. Phys.* **1978**, *69*, 5151−5162.
(16) Wadt, W. R.; Cartwright, D. C.; Cohen, J. S. *Appl. Phys. Lett.* **1977**, *31*, 672−674.
(17) Wadt, W. R. *J. Chem. Phys.* **1978**, *68*, 402−414.
(18) Wadt, W. R. *J. Chem. Phys.* **1980**, *73*, 3915−3926.
(19) Amarouche, M.; Durand, G.; Malrieu, J. P. *J. Chem. Phys.* **1988**, *88*, 1010−1018.
(20) Daskalopoulou, M.; Böhmer, H.-U.; Peyerimhoff, S. D. *Z. Phys. D* **1990**, *15*, 161−169.
(21) Whitaker, B. J.; Woodward, C. A.; Knowles, P. J.; Stace, A. J. *J. Chem. Phys.* **1990**, *93*, 376−383.
(22) Audouard, E.; Spiegelmann, F. *J. Chem. Phys.* **1991**, *94*, 6102−6124.
(23) Ma, N. L.; Li, W.-K.; Ng, C. Y. *J. Chem. Phys.* **1993**, *99*, 3617−3621.
(24) Gadéa, F. X.; Paidarová, I. *Chem. Phys.* **1996**, *209*, 281−290.
(25) Mášik, J.; Urban, J.; Mach, P.; Hubač, I. *Int. J. Quantum Chem.* **1997**, *63*, 333−343.
(26) Naumkin, F. Y.; Wales, D. J. *Mol. Phys.* **1998**, *93*, 633−648.
(27) Heidenreich, A.; Jortner, J. *J. Electron Spectrosc. Relat. Phenom.* **2000**, *106*, 187−197.
(28) Paidarová, I.; Gadéa, F. X. *Chem. Phys.* **2001**, *274*, 1−9.
(29) Ha, T.-K.; Rupper, P.; Wüest, A.; Merkt, F. *Mol. Phys.* **2003**, *101*, 827−838.
(30) Pernpointner, M.; Kryzhvoi, N. V.; Unbaczek, S. *J. Chem. Phys.* **2008**, *129*, 024304.
(31) Ng, C. Y.; Trevor, D. J.; Mahan, B. H.; Lee, Y. T. *J. Chem. Phys.* **1977**, *66*, 446−449.
(32) Dehmer, P. M.; Dehmer, J. L. *J. Chem. Phys.* **1978**, *68*, 3462−3470.
(33) Pratt, S. T.; Dehmer, P. M. *Chem. Phys. Lett.* **1982**, *87*, 533−538.
(34) Dehmer, P. M.; Pratt, S. T.; Dehmer, J. L. *J. Phys. Chem.* **1987**, *91*, 2593−2598.
(35) Tonkyn, R. G.; White, M. G. *J. Chem. Phys.* **1991**, *95*, 5582−5589.
(36) Lu, Y.; Matsui, T.; Tanaka, K.; Ito, K.; Hayaishi, T.; Morioka, Y. *J. Phys. B: At. Mol. Opt. Phys.* **1992**, *25*, 5101−5108.
(37) Pradeep, T.; Niu, B.; Shirley, D. A. *J. Chem. Phys.* **1993**, *98*, 5269−5275.
(38) Hall, R. I.; Lu, Y.; Morioka, Y.; Matsui, T.; Tanaka, T.; Yoshii, H.; Hayaishi, T.; Ito, K. *J. Phys. B: At. Mol. Opt. Phys.* **1995**, *28*, 2435−2451.
(39) Signorell, R.; Wüest, A.; Merkt, F. *J. Chem. Phys.* **1997**, *107*, 10819−10822.
(40) Signorell, R.; Merkt, F. *J. Chem. Phys.* **1998**, *109*, 9762−9771.
(41) Morioka, Y.; Tanaka, T.; Yoshii, H.; Hayaishi, T. *J. Chem. Phys.* **1998**, *109*, 1324−1328.
(42) Onuma, T.; Yoshii, H.; Ishijima, H.; Itou, Y.; Hayaishi, T.; Morioka, Y. *J. Mol. Spectrosc.* **1999**, *198*, 209−217.
(43) Signorell, R.; Hollenstein, U.; Merkt, F. *J. Chem. Phys.* **2001**, *114*, 9840−9851.
(44) Wüest, A.; Rupper, P.; Merkt, F. *Mol. Phys.* **2001**, *99*, 1941−1958.
(45) Rupper, P.; Merkt, F. *J. Chem. Phys.* **2002**, *117*, 4264−4281.
(46) Rupper, P.; Merkt, F. *Mol. Phys.* **2002**, *100*, 3781−3784.
(47) Yoshii, H.; Hayaishi, T.; Onuma, T.; Aoto, T.; Morioka, Y.; Ito, K. *J. Chem. Phys.* **2002**, *117*, 1517−1521.
(48) Fedor, J.; Parajuli, R.; Matt-Leubner, S.; Echt, O.; Hagelberg, F.; Gluch, K.; Stamatovic, A.; Probst, M.; Scheier, P.; Märk, T. D. *Phys. Rev. Lett.* **2003**, *91*, 133401.
(49) Wüest, A.; Merkt, F. *J. Chem. Phys.* **2004**, *120*, 638−646.
(50) Rupper, P.; Zehnder, O.; Merkt, F. *J. Chem. Phys.* **2004**, *121*, 8279−8290.
(51) Yoshii, H.; Tsukamoto, K.; Hayaishi, T.; Aoto, T.; Ito, K.; Morioka, Y. *J. Chem. Phys.* **2005**, *123*, 184303.
(52) Wüest, A.; Merkt, F. *Mol. Phys.* **2005**, *103*, 1285−1300.
(53) Vasilatou, K.; Hollenstein, U.; Merkt, F. *Mol. Phys.* **2010**, *108*, 915−926.
(54) Fedor, J.; Echt, O.; Gluch, K.; Matt-Leubner, S.; Scheier, P.; Märk, T. D. *Chem. Phys. Lett.* **2007**, *437*, 183−188.
(55) Carrington, A.; Gammie, D. I.; Page, J. C.; Shaw, A. M.; Hutson, J. M. *J. Chem. Phys.* **2002**, *116*, 3662−3669.
(56) Zehnder, O.; Mastalerz, R.; Reiher, M.; Merkt, F.; Dressler, R. A. *J. Chem. Phys.* **2008**, *128*, 234306.
(57) Cohen, J. S.; Schneider, B. *J. Chem. Phys.* **1974**, *61*, 3230−3239.
(58) Lefebvre-Brion, H.; Field, R. W. *The Spectra and Dynamics of Diatomic Molecules*; Elsevier: Amsterdam, 2004.
(59) Yamada, C.; Kanamori, H.; Hirota, E. *J. Chem. Phys.* **1985**, *83*, 552−555.
(60) Paul, Th. A.; Liu, J.; Merkt, F. *Phys. Rev. A* **2009**, *79*, 022505.
(61) Tang, K. T.; Toennies, J. P. *J. Chem. Phys.* **2003**, *118*, 4976−4983.
(62) Reiher, M. Relativistic Douglas−Kroll−Hess Theory. In *Wiley Interdisciplinary Reviews: Computational Molecular Science*; Wiley: New York, 2012; Vol. 2, pp 139−149.
(63) Roos, B. O.; Lindh, R.; Malmqvist, P.-A.; Veryazov, V.; Widmark, P.-O. *J. Phys. Chem. A* **2004**, *108*, 2851.
(64) Berning, A.; Schweizer, M.; Werner, H.-J.; Knowles, P. J.; Palmieri, P. *Mol. Phys.* **2000**, *98*, 267.
(65) Werner, H.-J.;et al. *MOLPRO*, version 2002.6; Cardiff University: Cardiff, Wales, 2002.
(66) Teachout, R. R.; Pack, R. T. *Atomic Data* **1971**, *3*, 195−214.
(67) Medved', M.; Fowler, P. W.; Hutson, J. M. *Mol. Phys.* **2000**, *98*, 453−463.
(68) Velchev, I.; Hogervorst, W.; Ubachs, W. *J. Phys. B: At. Mol. Opt. Phys.* **1999**, *32*, L511−L516.
(69) Hollenstein, U.; Seiler, R.; Merkt, F. *J. Phys. B: At. Mol. Opt. Phys.* **2003**, *36*, 893−903.
(70) Tanaka, Y.; Yoshino, K.; Freeman, D. E. *J. Chem. Phys.* **1973**, *59*, 5160−5183.
(71) The difference in the zero point energy of the two isotopomers $^{84}Kr_2$ and $^{84}Kr-^{86}Kr$ amounts to less than 0.01 cm^{-1} and so does the difference in the atomic ionization energies.[69]
(72) Wüest, A.; Merkt, F. *J. Chem. Phys.* **2003**, *118*, 8807−8812.

(73) Wörner, H. J.; Grütter, M.; Vliegen, E.; Merkt, F. *Phys. Rev. A* **2005**, *71*, 052504; See erratum in *Phys. Rev. A* **2006**, *73*, 059904(E).
(74) See EPAPS document no. E-JCPSA6-119-X018344 for a table of measured and calculated positions of all vibrational levels of the I(1/2u), I(3/2u), II(1/2u), I(1/2g), I(3/2g), and II(1/2g) states of $^{40}Ar_2^+$ and $^{36}Ar_2^+$ up to 2 cm^{-1} below the corresponding dissociation limits. This document may be retrieved via the EPAPS homepage (http://www.aip.org/pubservs/epaps.html) or from ftp.aip.org in the directory /epaps/. See the EPAPS homepage for more information.
(75) Moore, C. E. *Atomic Energy Levels*; NBS Circular 467/1 National Bureau of Standards: Washington, DC, 1949.
(76) Moore, C. E. *Atomic Energy Levels*; NBS Circular 467/2 National Bureau of Standards: Washington, DC, 1952.
(77) Moore, C. E. *Atomic Energy Levels*; NBS Circular 467/3 National Bureau of Standards: Washington, DC, 1958.